WARSAW UNIVERSITY OF TECHNOLOGY Index 351733
FACULTY OF CIVIL ENGINEERING
COMMITTEE FOR CIVIL AND WATER ENGINEERING
POLISH ACADEMY OF SCIENCES ISSN 1230-2945

DOI: 10.24425/ace.2025.154139
ARCHIVES OF CIVIL ENGINEERING
Vol. LXXI ISSUE 2 2025

pp. 591 –605

Research paper

Microstructure of calcium sulfoaluminate mortar with basalt additive at elevated temperature

Konrad A. Sodol[1], Sebastian Miszczak[2], Jacek Szer[3], Łukasz Kaczmarek[4]

Abstract: This article is motivated by ensure the fire safety of the building and deeper understanding on special cements under elevated temperature loads. Knowledge about influence of high temperatures on calcium sulfoaluminate cement (CSA) based materials has crucial impact on ensuring the fire safety of the buildings. CSA based composites are dedicated to special usage in demanding infrastructure constructions. As there is no or insufficient evidence on the influence of heat on calcium sulfoaluminate materials, this article is motivated to extend current literature knowledge on CSA microstructures at higher temperatures up to 800°C. Recognising the effect of high temperature is particularly important given the significant differences between CSA and Ordinary Portland Cement (OPC). Evidence shows influence of mixture proportion on composite structure, filler-matrix bond, and matrix behaviour during temperature exposure. Obtained results might help in understanding phenomena occurring within material under temperature load and determine next research directions in this area.

Keywords: basalt, calcium sulfoaluminate, CSA, high-temperature, microstructure

[1]PhD., Eng., Hydro Building Systems Poland, R&D Departament, ul. Rokicińska 211/217, 92-620 Lodz, Poland, e-mail: konrad.sodol@hydro.com, ORCID: 0000-0001-8129-1353
[2]PhD., Eng., Lodz University of Technology, Institute of Materials Science and Engineering, ul. Stefanowskiego 1/15, 90-537 Lodz, Poland, e-mail: sebastian.miszczak@p.lodz.pl, ORCID: 0000-0002-6074-9529
[3]Assoc. Prof., DSc., PhD., Eng., Lodz University of Technology, Department of Building Physics and Sustainable Design, Al. Politechniki 6, 93-590 Lodz, Poland, e-mail: jacek.szer@p.lodz.pl, ORCID: 0000-0002-7830-2952
[4]Prof., DSc., PhD., Eng., Lodz University of Technology, Institute of Materials Science and Engineering, ul. Stefanowskiego 1/15, 90-537 Lodz, Poland, e-mail: lukasz.kaczmarek@p.lodz.pl, ORCID: 0000-0002-6163-3608

1. Introduction

Cement is one of the most commonly used binding agents in civil engineering and has one of the biggest impact on carbon dioxide emission in building sector [1]. Due to the concern estimate of cement production contributing to an annual global CO_2 emission of 5–7%, it is essential to prioritize reducing carbon dioxide emissions in this sector of the economy. Calcium sulfoaluminate cement (CSA) are called „green binders" because of lower CO2 emission during production in comparison to Portland cements (OPC) [2]. This difference is due to the composition of clinker, which is based on bauxite, limestone, and gypsum. The production process requires less energy to grid sinter CSA clinker due to its lower hardness than OPC clinker. The interaction of water (H) with the CSA cement results in a highly expansive hydraulic binder. Main hydrated phases are: ettringite (C6AŠ3H32), monosulfite (C4AŠH12), aluminium hydroxide (AH3), stratlingite (C2ASH8) [3]. However, inert phases might occur e.g. perovskite(s). The hydration process of CSA cement, mainly ye'elemite with gypsum, is shown in Fig. 1 and it is described in Table 1.

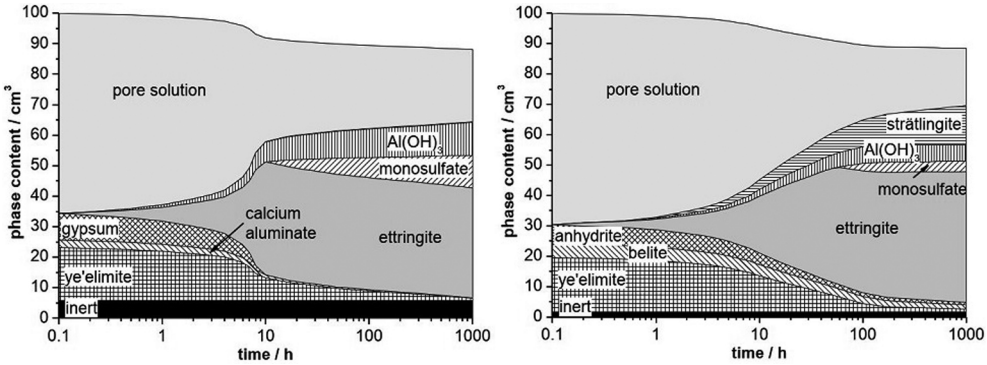

Fig. 1. Examples of hydration modelling of CSA cements [3]

Table 1. Example of CSA cement hydration process [4]

C4A3Š + (x + 6)H → C4AŠH12 + 2AH3	(1)
C4A3Š + 2CŠH2 + 34H → C6AŠ3H32 + 2AH3	(2)
C4A3Š + 8CŠH2 + 6CH + 74H → 3C6AŠ3H32	(3)
C2S + AH3 + 5H → C2ASH8	(4)
2C2S + (2 – a + b)H → CaSHb + (2 – a)CH	(5)

Description: "x" represents a variable amount of water that combines with the compound C4AŠH12; "a" and "b" indicate the stoichiometry of the hydrates that might be formed. For instance, "a" may represents the amount of a specific component (e.g. water) that is less than the maximum amount that can be bound in the hydration process, and "b" may represents a variation of water content in the belite phase of the cement.

Due to phase behavior in limited freedom of deformation, as expansive material, CSA cement may indicate increased tightness against moisture, water, gas, and petroleum permeation. This results in sealing of horizontal and vertical joints and connections, therefore, expansive cements-based composites are recommended to: joints in shell cylindrical tanks (wastewater clarifiers, water settlers, sewage, and water pumping stations), industrial ceilings (because of resistance to petroleum products, aggressive environment of gaseous products, technological liquids), bridge carriageways, roadways, airport aprons, etc. [5].

Other thermal properties of CSA cements can also be exploited, e.g. the reversible reaction of ettringite can be used to accumulate energy in heat storage battery [6, 7], while the high enthalpy of the CSA-based materials can be utilized for passive fire protection in metal associated structures e.g.: facades, doors, etc. [8].

The external heat field acting on the cement composite has a significant effect on physic-ochemical changes in each of its elements, e.g.: matrix [9], fillers, and aggregate [10, 11]. Tchekwagep et al. [12], considering the influence of the temperature (up to 300°C) on porosity of CSA concrete, showed that the porosity of the concrete increases with increasing temperature due to the loss of physically and chemically bound water. Above 100°C chemically bound water evaporates and the porosity change between 100 and 200°C was in linear trend line. At 300° C, the pore structure was "greatly damaged" – an increase in the volume of large pores, described as macropores, was observed. Tchekwagep and co-authors indicated that the linear relationship between temperature-related mass loss and total porosity aligns closely with an R-squared value of 0.98 to the Gawin model, which suggests that the loss of chemically bound water with temperature changes. This correspondence was established through a comparison of experimental data based on three-point nitrogen absorption data tests against the linear predictions of the Gawin model [13]. In another study Tchekwagep et al. [14] showed that CSA-based concrete (cement : aggregate : water : retarder – 1:4,2 : 0,01 : 0,04 ratio) has porous network of empty spaces with diameter of 2–50 nm, where, as they point, there is possible occurrence of nano-pores < 2 nm and micro-pores >50 nm. During heating up to 100°C, the size of the pore structure (BET method: average pore diameter) was 14.5 nm, at 200°C – 9.9 nm, and at 300°C it was 12 nm. Tchekwagep et al. [15] also used the in situ High Temperature XRD (HT-XRD) method to investigate the CSA paste (cement : water – 1:0,4) crystal structure in the temperature range between 20 and 70°C. It was found that the crystal structure of CSA undergoes a transformation from a cubic to an orthorhombic form, which is highly significant for understanding and analyzing research on heterophases (DTG/TG curve). Sodol et al. [8] indicated that up to 600°C total sum of enthalpy of CSA paste ($\Delta H_{Sum,600°C,CSA}$ = 647,3 J/g) was 2.5×higher than that of OPC CEM I 42.5R paste ($\Delta H_{Sum,600°C,OPC}$ = 246,3 J/g). Microscopy examination proved that structure of CSA paste (w/c = 0.5) had defects (e.g. cracks) at 23°C and during high temperature exposure (up to 800°C) the structure might undergo re-sintering. In another work by Sodol et al. [17] this phenomenon was observed at temperatures between 600–800°C. Dehydrating of cement phases was also analyzed by Kaufman et al. [6] and Collier [16]. The most relevant dehydration and dehydroxylation processes with regard to the degradation of CSA based materials are shown in Table 2.

The influence of high temperature on different concrete aggregates was analysed by Biro and Lublóy [18]. They found that the size and strength of the aggregates can change because

Table 2. CSA paste dehydration and dehydroxylation general process [6, 16]

Temperature load	Phase changes
from 90°C	Ettringite dehydration
from 150°C	Monosulfate partially dehydration
200–250°C	Stratlingite dehydration
200–300°C	Alumina dihydroxide dehydroxylation
from 450°C	Monosulfate fully dehydration

of the external heat load, and one of the most stable is basalt. This feature of basalt was already indicated in the 1970s extensive studies on rock metallurgy and the effect of temperature on basalt rocks conducted by Wyszomirski and Stoch [20]. Also Khoury [19] dividing aggregates by type of their thermic reactions listed basalt as thermally stable aggregate. In addition to its thermal properties, the use of the fine fraction of basalt rock can be recommended for the special production of building materials due to the improvement in workability [21]. Such combination of CSA cement and basalt filler can be used as inter-layer material for recycled aggregate [22]. Tchekwagep et al. [23] investigated the effect of river sand, basalt, and artificial sand, as well as various cooling methods, on the engineering characteristics of CSA mortar. They emphasize that the rapid cooling effect of water immersion cooling promotes the formation of a new hydrated crystal structure when a dehydration reaction occurs, CaO decomposes, and SiO_2 becomes active after being exposed to high temperatures. Previous study by Tchekwagep et al. [24] indicates that basalt may provide advantages due to its compressive strength. Upon examining a breakthrough specimen at higher temperatures (up to 300°C), an increase in observed cracks and formation of new pores occurred.

Even comprehensive literature reviews, such as that of Sundin et al. [25], indicate a lack of evidence on the effect of high temperatures on CSA-based materials containing basalt additives. The aim of this publication is to enhance knowledge about changes in the microstructure of CSA-basalt mortars under high temperatures (23°C, 300°C, 600°C, 800°C) and to identify areas of investigation that could be explored in further research.

2. Experimental

2.1. Materials

Calcium sulfoaluminate cement (commercial name: AliCem Green from Heidelberg; cement/gypsum ratio 3:1) was used to prepare mortar samples. Chemical composition of CSA cement is shown in Table 3.

As a second ingredient, mechanically crushed finest (0/0.063) nepheline basalt was used. The origin of basalt was Lower Silesian opencast mine Krzeniów deposit, Poland. Chemical composition of basalt powder is shown in Table 4.

Table 3. Chemical composition of calcium sulfoaluminate cement (AliCem Heidelberg)

Component	SiO_2	Al_2O_3	CaO	Fe_2O_3	MgO	K_2O	Na_2O	SO_3	TiO_2
Wt. %	6.89	23.74	43.06	1.11	2.70	0.68	1.01	20.37	0.44

Table 4. Chemical composition of basalt powder [26]

Component	SiO_2	Al_2O_3	CaO	Fe_2O_3	MgO	P_2O_5	TiO_2	K_2O	Na_2O	MnO	(SO_3)	(Cl)	(F)
Wt. %	42.08	11.80	10.03	13.69	13.25	0.72	2.54	1.30	3.36	0.22	<0.01	0.14	<0.01

Other components: ~1%

The chemical composition characteristics were provided by the manufacturer and do not differ significantly from the historical data provided by Wyszomirski and Stoch [20]. Phase composition of basalt from Krzeniów deposit was identified based on the XRD pattern obtained by Wyszomirski and Szydłak [27]. For the purpose of this paper, the titanomagnetite (Tm) was marked based on XRD patterns made by Wen et al. [28]. A reproduced diffraction pattern with highlighted identified crystalline phases is provided in Fig. 2. Main identified minerals in this raw material were nephelines, olivines, plagioclases and titanomagnetite.

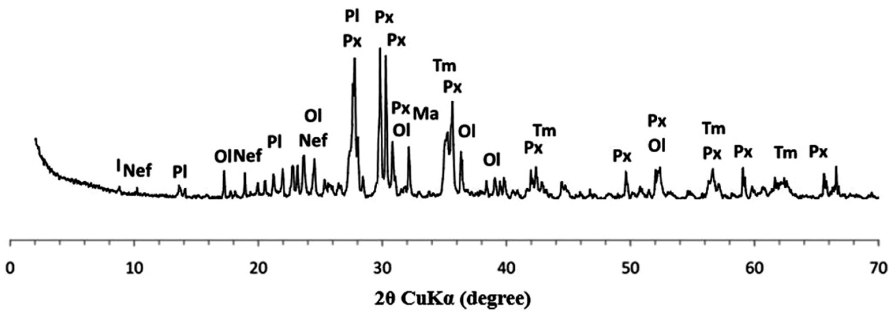

Fig. 2. XRD pattern of basalt powder from Krzeniów deposit [27, 28]; description: I – illite, Ol – olivine, Nef – nepheline, Pl – plagioclase, Px – pyroxene, Ma – magnetite, Tm – titanomagnetite

2.2. Sample preparation

Specimens were prepared by blending of CSA cement and basalt powder mixture with water. Samples with two different proportions of components were prepared, their composition ratios are presented in Table 5.

Table 5. Samples composition

Composition	**Cement : basalt : water, [wt.]**
B20	1 : 0.2 : 0.5
B40	1 : 0.4 : 0.5

The first step in sample preparation was to mix the dry ingredients. Weighted reagents were poured into 20-liter plastic bucket, then they were mixed for 3 minutes at I-level of speed (80 rpm) of hand electric stirrer (MacAllister 1200W). The resulting mixture was then combined with water (having a temperature of about 10°C) and stirred with a hand electric stirrer (MacAllister 1200 W) until a homogeneous semi-fluid suspension was obtained. Thus prepared mortar was poured into moulds (dimensions: $10 \times 10 \times 40$ mm) and subjected to vibration, removing any excess. To prevent water evaporation, the specimens were secured by wet gauze swab and filter paper and left for 24h. Next, specimens were demoulded and treated in a 100% humidity environment (wet conditioning) at the room temperature for 6 days. After this, the samples were treated in 65 ± 5% humidity environment for 21 days (air-wet conditioning). Finally, 28-day-old samples were heat-treated in an atmosphere oven (NEOTherm, Zakład Elektromechaniczny, Wrocław, Polska). The heat-treatment regime, including: heating rate, isothermal heating, cooling rate, was maintained in accordance with previous research [17]). A total of 4 sets of samples were prepared in this way. The parameters of heat-treatment are shown in Table 6.

Table 6. Parameters of specimens' heat treatment

Heat-treatment temperature (maximal)	Heating rate	Isothermal heating	Cooling rate
300°C, 600°C, 800°C	5°C/min	2 h	with furnace

After heat-treatment, samples were mechanically divided into smaller parts and dry-grinded using SiC sandpapers with gradation up to 800. After grinding the specimens were cleaned by compressed air.

2.3. Methods

Internal microstructure of samples was assessed by scanning electron microscopy (SEM) using JEOL JSM-6610 microscope (JEOL Ltd., Tokyo, Japan) operating in BSE mode at 20–25 kV accelerating voltages. Additionally, EDS module JEOL JED-2300 was used for mapping and identification of structural components. Microscopic investigations were made on the inner cross-sectional areas of the samples, approximately 10 mm from the outer edges. SEM observations and EDS analyses were conducted in high vacuum mode, without the use of an additional conductive coating. Obtained images were analysed using 2D CAD image processing software provided by Autodesk®Inc. The measured dimensions were proportional to the scale of the SEM images.

3. Results and discussion

The SEM/EDS results are presented in the form of microstructure images accompanied by a collection of color-coded EDS maps indicating the distribution of specific elements. Due to the multitude of utilized map elements, the general principle is as follows: against

a black background, the dispersion of each element is indicated by a corresponding colour and identified in the title above image. Depending on the concentration of the particular element, individual points or entire fields of their clusters may appear on the map.

3.1. B20 composition

Cross-section SEM images and EDS maps of B20 composition sample treated in typical ambient temperature (23°C) are shown in Fig. 3.

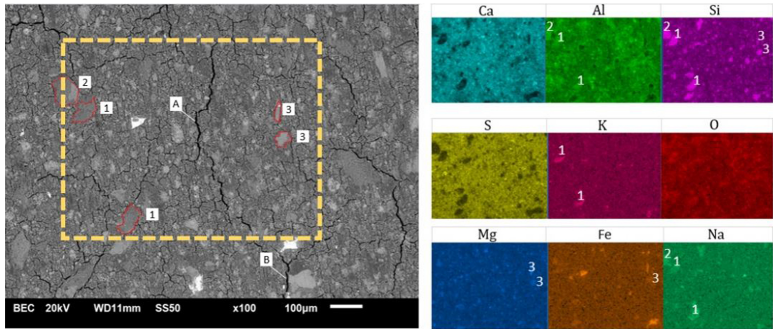

Fig. 3. Microstructure of nepheline (1), plagioclase (2), and olivine (3) in B20 composition treated at 23°C

The main identified phases, based on the EDS analyses, were nepheline (1), plagioclase (2), and olivine (3). The sample had structure with highly visible grains and numerous internal cracks. The visible cracks were mainly in the cement matrix and were continuous in nature. The widest observed cracks were in matrix (A) – 6.1 µm, in matrix-filler border (B) – 6.8 µm. No significant cracking was observed in area of olivines. Defects was located, mainly, in the matrix – at nephelines or plagioclases borders.

Figure 4 shows more detailed microstructure of B20 composition sample treated at 23°C. The titanomagnetite (1), pyroxene – augite (2), and olivine (3) phases were identified. A significant number of cracks in the matrix can be seen. The cracks were in contact with filler grain and were approx. 1 µm thick.

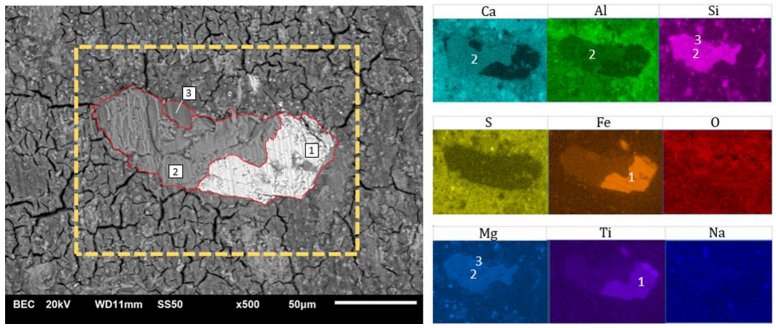

Fig. 4. Microstructure of titanomagnetite (1), pyroxene-augite (2), and olivine (3) in B20 composition treated at 23°C

Figure 5 shows microstructure of B20 composition treated at 300° C. It can be seen that the temperature has a significant effect on the microstructure compared to the sample treated at ambient conditions. In addition to barely visible cracks, numerous pores can be observed. Their sizes were between 3 and 8 μm (e.g. A – 3.4 μm; B – 6.3 μm; C – 3.8 μm). The microstructure contained two main components of the basalt aggregate: calcium phosphate (1) and pyroxene (2). The phosphorus phase is rare component of nepheline basalt, its content was 0.72% wt. (as referred in Table 4).

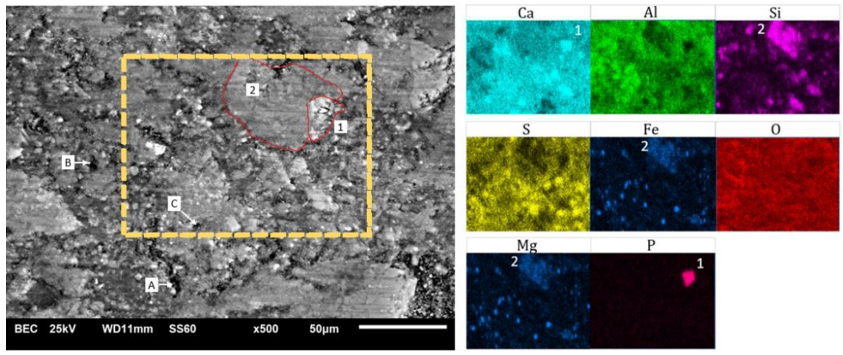

Fig. 5. Microstructure of calcium phosphate (1) and pyroxene (2) in B20 composition treated at 300°C

Microstructure of B20 composition treated at 600°C is shown in Fig. 6. The main components were titanomagnetite (1) and pyroxene (2, 3) phases. Lower temperatures defects, as cracks presented in previous figures, were not observed at 600°C. Thermal treatment at 600°C resulted in partial resintering of cement matrix and the disappearance of the cracks. In the Fig. 6, the investigated defects were pores, where their sizes were between 3.5 μm (A) and 22.7 μm (B). The basalt filler particles do not appear to resinter as a cement matrix. Nevertheless, the structure appears to be healed from cracks and gaps by high temperature.

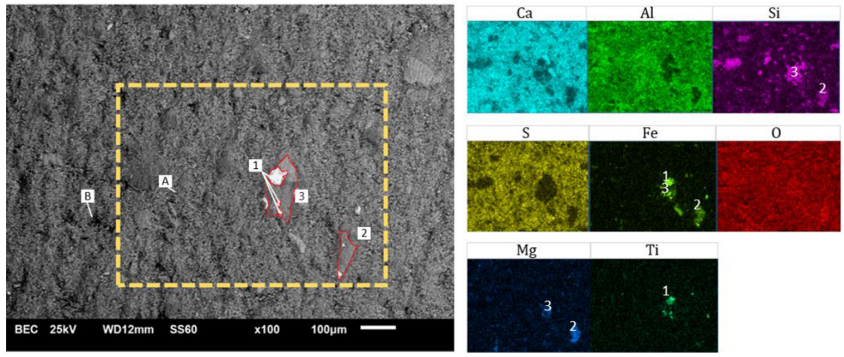

Fig. 6. Microstructure of titanomagnetite (1) and pyroxene (2), (3) in B20 composition treated at 600°C

Microstructure and EDS analysis of B20 composition treated at 800°C are shown in Fig. 7. There are no obvious cracks or discontinuities in the observed structure, except for pores of various sizes from 2 μm (A) up to 20 μm (B). Main identified phase was plagioclase and olivine spinel (1). Similarly to the sample annealed at 600°C, microstructure appears to be resintered and healed.

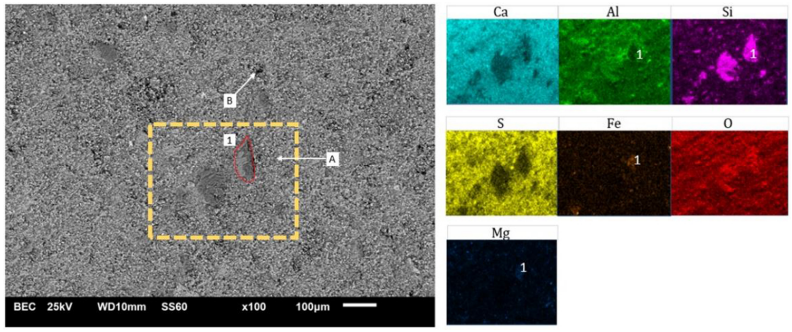

Fig. 7. Microstructure of spinel plagioclase and olivine phase (1) in B20 composition treated at 800°C

The structure (1) observed in Fig. 7 was subjected to a more detailed analysis. An enlarged view of this structure is shown in Fig. 8. It consists of plagioclase (1) and olivine (2). It can also be seen that the heat treatment has made the cement matrix fine-grained and well bonded to the spinel phases, except for single discontinuities e.g. 5.6 μm crack (C).

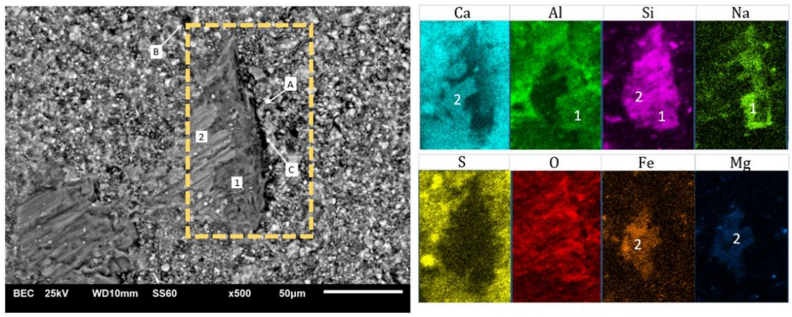

Fig. 8. Microstructure of spinel plagioclase (1) and olivine (2) phase in B20 composition treated at 800°C

3.2. B40 composition

The SEM/EDS analysis of samples made of B40 composition were performed in the same way as for B20 composition. SEM images and EDS analysis of B20 sample treated at ambient temperature (23°C) are shown in Fig. 9.

In Fig. 9, the conducted EDS analysis allowed to identify olivine (1) and nepheline (2) phases. Numerous cracks with a width of 3.5 μm (A) to 4 μm (D) can be seen in the cement matrix. The matrix-grain interface was continuous and well bonded. However, in marked locations, the deviations were observed, e.g. in (B) point. Between matrix and olivine (1) the material loss was observed with 1μm width. Similar deviation was found for nepheline, where material loss had ~1,5 μm (C) width.

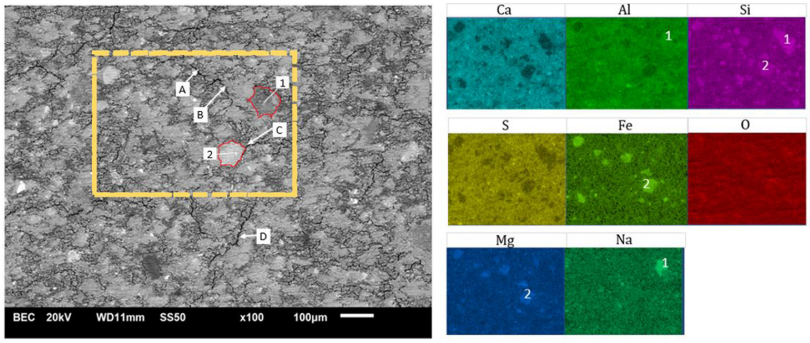

Fig. 9. Microstructure of olivine (1) and nepheline (2) in B40 composition treated at 23°C

Due to the increased filler content in the B40 composition compared to the B20, the number of visible cracks is reduced, as shown in Fig. 10. Olivine (1) had continuous structure without visible defects. Furthermore, the crack (E) defect was observed in matrix and not in the filler grains, the approximate width of matrix crack was ~2 µm. However, the proper bond between the basalt filler and cement was locally defected, with crack (F) width in the range of 1.4 µm.

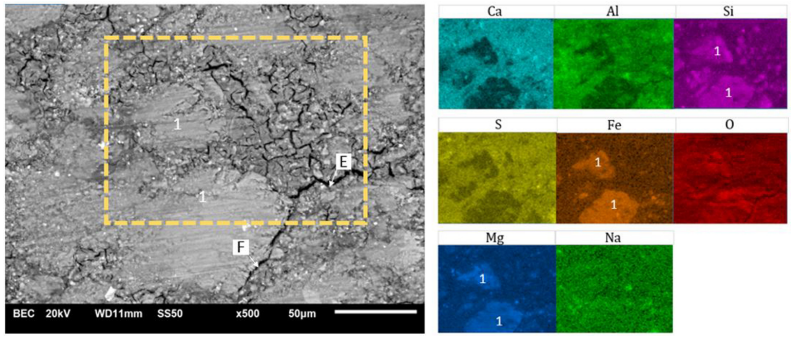

Fig. 10. Microstructure of olivine (1) in B40 composition treated at 23°C

Figure 11 shows the microstructure and EDS of B40 composition treated at 300°C. The main identified phases are titanomagnetite spinel (1) and plagioclase (2). The boundaries between these phases and the matrix were compact and free of discontinuities. Only in a few places, on the border of matrix and titanomagnetite, small defects (G) less than 2 µm wide were observed.

In Fig. 12, the microstructure and EDS analysis of cement with basalt filler composition treated at 600°C is shown. Three main types of filler can be distinguished: olivine (1), plagioclase (2), and titanomagnetite (3). Quantitatively, the olivine phases with the addition of plagioclase predominates. In their background, titanomagnetite inclusions of 8–12 µm in size are visible. Pores ranging in size from 8 µm (A) to 30 µm (B) can also be seen, but overall the microstructure is fairly uniform – most likely as a consequence of resintering at the filler-matrix interfaces.

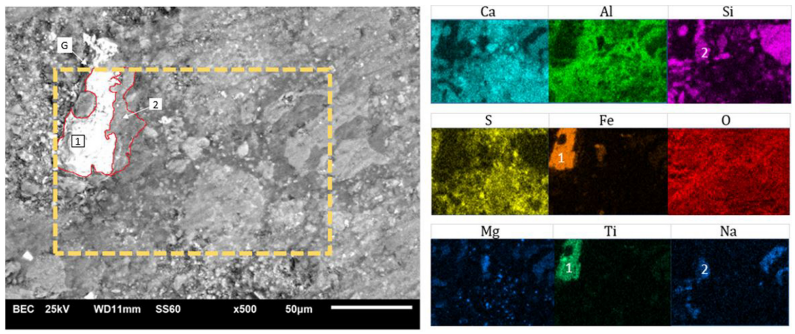

Fig. 11. Microstructure of spinel titanomagnetite (1) and plagioclase (2) phase in B40 composition treated at 300°C

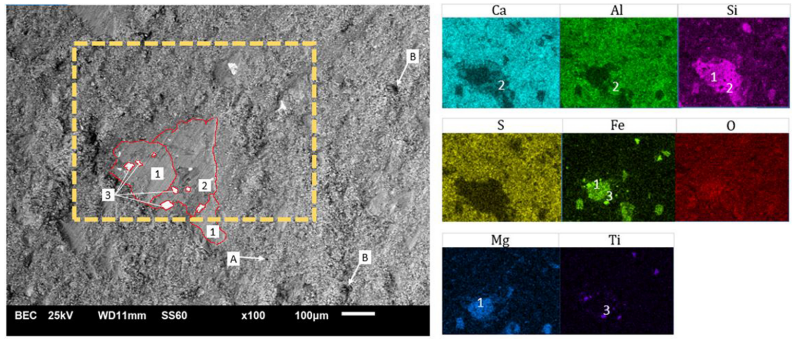

Fig. 12. Microstructure of olivine (1), plagioclase (2), and titanomagnetite (3) in B40 composition treated at 600°C

Figure 13 shows microstructure of B40 proves fine-grained structure of material after 800°C treatment. Furthermore, porosity of material is irregular. The range of pores are between 4.3 μm (M), and 29.4 μm (L). Cement matrix in titanomagnetite border is continuous and without any defects.

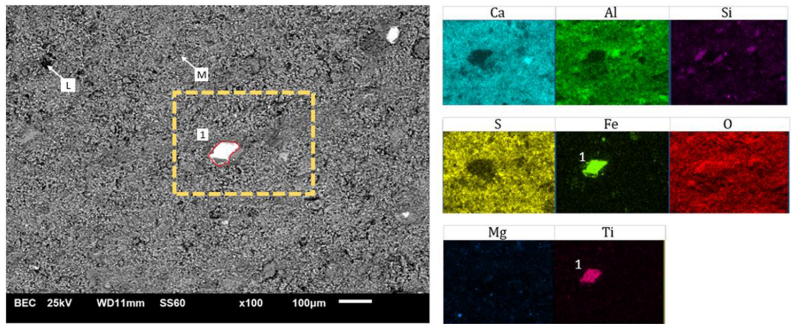

Fig. 13. Defects of material and microstructure of titanomagnetite (1) in B40 composition treated in 800°C

3.3. The comparison of research results

Even a cursory analysis of the SEM images and EDS element distribution maps shows significant differences in the internal structure of the samples. Table 7 summarizes the occurrence and number of structural defects (microcracks and porosities) observed in samples annealed at different temperatures and with different initial compositions.

Table 7. Comparison of material defects based on microstructure data

Max. treatment temperature	B20	B40
23°C (ambient)	Micro-cracks: numerous Cracks width (matrix): 6.1–6.8 μm, Cracks width (matrix–filler): ~1 μm. Pores: none	Micro-cracks: numerous Cracks width (matrix): 2–4 μm, Cracks width (matrix – filler): 1–1.4 μm. Pores: none
300°C	Micro-cracks: numerous Cracks: matrix–filler – barely visible Pores: numerous Pores size: 3–8 μm.	Micro-crack: few Cracks: matrix – filler: <2 μm Pores: few
600°C	Micro-cracks: none Cracks: none Pores: numerous Pores size: 3.5–22.7 μm.	Micro-crack: none Cracks width (matrix): 6.1–25.8 μm Pores: numerous Pores size: 8–30 μm.
800°C	Micro-cracks: single Crack width (matrix–filler): 5.6 μm Pores: numerous Pores size: 2–20 μm	Micro-cracks: none Pores: numerous Pores size: 4.3–29.4 μm

Presented data shows that in 23°C an increase in the amount of basalt filler can reduce the size of the pores and capillary network. However, as the water content in the dry mix decreases, the workability (understood as ability to mix) also decrease, which can be crucial from an industrial point of view. Up to 300°C, size of discontinuities at the matrix-filler border was at a similar level, between 1 and 1.5 μm. After treatment at 600°C, an increase in porosity was observed with a reduction in the number of cracks. Furthermore, in this level of heat treatment the highest found pore had 30 μm. After 800°C treatment, in B20 composition cracks size decreased and microcrack in matrix – aggregate appeared in size of 5,6 μm. For B40 pores were in ranges 4,3–29,4 μm. The data presented suggests that re-sintering occurs above 600°C in a comparable way to CSA compositions without fillers, as observed by Sodol et al. [17].

4. Summary and conclusions

The study carried out in this paper aimed to determine the effects of elevated and high temperatures on the internal structure of calcium sulfoaluminate cement (CSA). The results showed a significant influence of the proportion of mortar components and the annealing temperature on the microstructure evolution of CSA cement with basalt addition.

– CSA cements containing a higher amount of basalt filler addition (B40 samples) were characterised by a smaller cracks' width, while maintaining the continuity of the matrix-grain interface. This may indicate a positive effect of the basalt filler addition on the defect rate of the cement mortar at ambient temperatures.
– In the microstructure of specimens annealed at 300 °, the appearance of numerous porosities because of material dehydration was observed. On the other hand, higher content of fine-grained basalt filler in B40 samples correlated with much lower porosity of the cement microstructure at temperatures up to 300°. Further research in this area is needed.
– Heat treatment of the B20 and B40 compositions at 600°C resulted in the increase in pore width but a reduction in the number of cracks. This can be attributed to the initiation of resintering process.
– After heat treatment conducted at 800°C both B20 and B40 CSA compositions had a similar microstructure, with quite a few small porosities within the matrix, but without cracks or discontinuities. The reduction in the size of the porosities and the disappearance of the cracks indicate the progress of the resintering process leading to the healing of the microstructure.

The findings presented above extend the current knowledge of CSA-based materials and their behaviour at high temperatures. The lack of similar information in current databases indicates the need for further research, which will be focused on the strength, porosity, and permeability properties at high temperatures.

References

[1] K. Zima, "Integrated analysis of costs and amount of greenhouse gases emissions during the building lifecycle", *Archives of Civil Engineering*, vol. 67, no. 2, pp. 413–423, 2021, doi: 10.24425/ace.2021.137176.

[2] L. Coppola, D. Coffetti, E. Crotti, G. Gazzaniga, and T. Pastore, "An Empathetic Added Sustainability Index (EASI) for cementitious based construction materials", *Journal of Cleaner Production*, vol. 220, pp. 475–482, 2019, doi: 10.1016/j.jclepro.2019.02.160.

[3] F. Winnefeld, M. Ben Haha, and B. Lothenbach, "Hydration mechanisms of calcium sulfoaluminate cements assessed by scanning electron microscopy and thermodynamic modelling", presented at the 13th International Congress on the Chemistry of Cement, 3-8 July 2011, pp. 1–7, Madrit, Spain, 2011.

[4] HEIDELBERG CEMENT Group, *Vademecum Technologa Betonu*. p. 3, 2017.

[5] W. Tur and M. Król, *Beton ekspansywny*. Arkady, 1999.

[6] J. Kaufmann, F. Winnefeld, and B. Lothenbach, "Stability of ettringite in CSA cement at elevated temperatures", *Advances in Cement Research*, vol. 28, no. 4, pp. 251–261, 2016, doi: 10.1680/jadcr.15.00029.

[7] B. Chen, K. Johannes, M. Horgnies, V. Morin, and F. Kuznik, "Characterization of an ettringite-based thermochemical energy storage material in an open-mode reactor", *Journal of Energy Storage*, vol. 33, art. no. 102159, 2021, doi: 10.1016/j.est.2020.102159.

[8] K.A. Sodol, Ł. Kaczmarek, and J. Szer, "Fire-temperature influence on Portland and calcium sulfoaluminate blend composites", *Materials*, vol. 13, no. 22, pp. 1–16, 2020, doi: 10.3390/ma13225230.

[9] I. Hager, T. Tracz, M. Choińska, and K. Mróz, "Effect of cement type on the mechanical behavior and permeability of concrete subjected to high temperatures", *Materials*, vol. 12, no. 18, 2019, doi: 10.3390/ma12183021.

[10] I. Hager, "Behaviour of cement concrete at high temperature", *Bulletin of the Polish Academy of Sciences: Technical Sciences*, vol. 61, no. 1, pp. 145–154, 2013, doi: 10.2478/bpasts-2013-0013.

[11] I. Hager, T. Tracz, J. Śliwiński, and K. Krzemień, "The influence of aggregate type on the physical and mechanical properties of high-performance concrete subjected to high temperature", *Fire and Materials*, vol. 40, no. 5, pp. 668–682, 2016, doi: 10.1002/fam.2318.

[12] J.J.K. Tchekwagep, P. Zhao, S. Wang, S. Huang, and X. Cheng, "The impact of changes in pore structure on the compressive strength of sulphoaluminate cement concrete at high temperature", *Materials Science-Poland*, vol. 39, no. 1, pp. 75–85, 2021, doi: 10.2478/msp-2021-0006.

[13] D. Gawin, F. Pesavento, and B.A. Schrefler, "What physical phenomena can be neglected when modelling concrete at high temperature? A comparative study. Part 1: Physical phenomena and mathematical model", *International Journal of Solids and Structures,* vol. 48, no. 13, pp. 1927–1944, 2011, doi: 10.1016/j.ijsolstr.2011.03.004.

[14] J.J.K. Tchekwagep, S. Wang, A.K. Mukhopadhyay, S. Huang, and X. Cheng, "Strengths of sulfoaluminate cement concrete and ordinary Portland cement concrete after exposure to high temperatures", *Ceramics-Silikáty,* vol. 64, no. 2, pp. 227–238, 2020, doi: 10.13168/cs.2020.0012.

[15] J.J.K. Tchekwagep, Y. Fengzhen, S. Wang, P. Zhao, S. Huang, and X. Cheng "Analysis of the phases and functions of the various compounds of calcium sulfoaluminate cement after exposure to high temperature", *Journal of Materials Research and Technology*, vol. 25, pp. 4154-4170, 2023, doi: 10.1016/j.jmrt.2023.06.215.

[16] N.C. Collier, "Transition and decomposition temperatures of cement phases – a collection of thermal analysis data", *Ceramics – Silikáty*, vol. 60, no. 4, pp. 338–343, 2016, doi: 10.13168/cs.2016.0050.

[17] K.A. Sodol, Ł. Kaczmarek, J. Szer, S. Miszczak, and M. Stegliński "Impact of Elevated Temperatures on Strength Properties and Microstructure of Calcium Sulfoaluminate Paste Impact of Elevated Temperatures on Strength Properties and Microstructure of Calcium Sulfoaluminate Paste", *Materials*, vol. 14, no. 22, art. no. 6751, 2021, doi: 10.3390/ma14226751.

[18] A. Biró and É. Lublóy, "Classification of aggregates for fire", *Construction and Building Materials*, vol. 266, Part A, 2021, doi: 10.1016/j.conbuildmat.2020.121024.

[19] G.A. Khoury, *Effect of Heat on Concrete*. London, 1995.

[20] P. Wyszomirski and L. Stoch, *Surowce i technologia hutnictwa skalnego.* Warszawa: Wydawnictwo Geologiczne, 1976.

[21] P. Wyszomirski, T. Szydłak, and T. Zawadzki, „The basaltic raw materials from the Rutki and Ligota Tułowicka deposits (Opole Province) and the directions of their possible use", *Zeszyty Naukowe Instytutu Gospodarki Surowcami Mineralnymi i Energią Polskiej Akademii Nauk*, no. 100, pp. 295–312, 2017.

[22] H. Zhang, T. Ji, et al., "Modifying recycled aggregate concrete by aggregate surface treatment using sulphoaluminate cement and basalt powder", *Construction and Building Materials*, vol. 192, pp. 526–537, 2018, doi: 10.1016/j.conbuildmat.2018.10.160.

[23] J.J.K. Tchekwagep, Z. Wang, S. Wang, S. Huang, and X. Cheng, "The influence of different fine aggregate and cooling regimes on the engineering properties of sulphoaluminate cement mortar after heating", *Case Studies in Construction Materials*, vol. 18, 2023, doi: 10.1016/j.cscm.2023.e01866.

[24] J.J.K. Tchekwagep, Z. Wang, Y. Fengzhen, et al., "The ability of different types of sand to preserve the integrity of calcium sulfoaluminate cement cement mortar during exposure to elevated temperatures", *Materials Science-Poland*, vol. 40, no. 4, pp. 64–77, 2022, doi: 10.2478/msp-2022-0044.

[25] M. Sundin, H. Hedlund, and A. Cwirzen, "Eco-Concrete in High Temperatures", *Materials*, vol. 16, no. 12, art. no. 4212, 2023, doi: 10.3390/ma16124212.

[26] Institute of Mechanised Construction and Rock Mining, Research protocol, '13985/NL/R/17', 2017, [unpublished].

[27] P. Wyszomirski and T. Szydłak, "Fine grain fraction from basalt processing and their usefulness in ceramics", *Mining Science – Mineral Aggregates*, vol. 23, no. 1, pp. 201–213, 2016, doi: 10.5277/mscma1622319.

[28] Y. Wen, X. Wen, J. Chen, J. Kuang, Q. Tang, Y. Tian, J. Fu, W. Huang, and T. Qiu, "Preparation of Direct Reduced Iron and Titanium Through Carbothermic Reduction-Magnetic Separation", *Materials*, vol. 7, no. 11, pp. 1–10, 2017, doi: 10.3390/min7110220.

Mikrostruktura zaprawy z cementu wapniowo-siarczano-glinianowego z wypełniaczem bazaltowym w wysokich temperaturach

Słowa kluczowe: Cement wapniowo-siarczano-glinianowy, bazalt, wysoka temperatura, CSA, mikrostruktura

Streszczenie:

Artykuł ten jest motywowany zapewnieniem bezpieczeństwa pożarowego budynków oraz głębszym zrozumieniem specjalnych cementów pod obciążeniem temperaturowym. Wiedza na temat wpływu wysokich temperatur na materiały na bazie cementu wapniowo-siarczano-glinianowego (CSA) jest kluczowa dla zapewnienia bezpieczeństwa pożarowego. Kompozyty na bazie CSA są przeznaczone do specjalnego zastosowania w wymagających konstrukcjach infrastrukturalnych. Ponieważ brakuje badań na temat wpływu ciepła na materiały na bazie CSA, niniejszy artykułma na celu poszerzenie aktualnej wiedzy literaturowej na temat mikrostruktur tych materiałów w temperaturach do 800°C. Rozpoznanie wpływu wysokiej temperatury jest szczególnie ważne, biorąc pod uwagę znaczące różnice między CSA a zwykłym cementem portlandzkim (OPC). Artykuł ten wskazuje na wpływ proporcji mieszanki na strukturę kompozytu, wiązanie wypełniacz–matryca i zachowanie matrycy podczas ekspozycji na temperaturę. Uzyskane wyniki mogą pomóc w zrozumieniu zjawisk zachodzących w materiale pod obciążeniem temperaturowym oraz określić dalsze kierunki badań.

Received: 2024-05-16, Revised: 2024-05-21